

# COSMIC REIONIZATION ON COMPUTERS: THE FAINT END OF THE GALAXY LUMINOSITY FUNCTION

NICKOLAY Y. GNEDIN<sup>1,2,3</sup>  
Draft version July 19, 2022

## ABSTRACT

Using numerical cosmological simulations completed under the ‘‘Cosmic Reionization On Computers’’ (CROC) project, I explore theoretical predictions for the faint end of the galaxy UV luminosity functions at  $z \gtrsim 6$ . A commonly used Schechter function approximation with the magnitude cut at  $M_{\text{CUT}} \sim -13$  provides a reasonable fit to the actual luminosity function of simulated galaxies. When the Schechter functional form is forced on the luminosity functions from the simulations, the magnitude cut  $M_{\text{CUT}}$  is found to vary between  $-12$  and  $-14$  with a mild redshift dependence. An analytical model of reionization from Madau, Haardt & Rees (1997), as used by Robertson et al. (2015), provides a good description of the simulated results, but only if the redshift dependence of the effective escape fraction (induced by physical processes not captured by the Madau, Haardt & Rees model) is accounted for.

*Subject headings:* cosmology: theory – cosmology: large-scale structure of universe – galaxies: formation – galaxies: intergalactic medium – methods: numerical

## 1. INTRODUCTION

It is well established by now that dwarf galaxies contribute significantly to the overall budget of ionizing photons during cosmic reionization, and that the slope of the Schechter function fit to the observational measurements of galaxy UV luminosity functions can approach and even exceed  $-2$  (Bouwens et al. 2011; Oesch et al. 2012; Bradley et al. 2012; Schenker et al. 2013; Willott et al. 2013; Oesch et al. 2013, 2014; Weisz et al. 2014; Bowler et al. 2014; Robertson et al. 2015; Atek et al. 2015b; Song et al. 2015; Finkelstein et al. 2015; Atek et al. 2015a). At the slope value of  $-2$  the total luminosity density of the Schechter fit diverges, so the Schechter function can remain a valid approximation to the actual galaxy luminosity function only over a limited range of luminosities. A commonly used resolution of this difficulty is to introduce a cutoff luminosity or magnitude  $M_{\text{CUT}}$  to the Schechter approximation (Robertson et al. 2013a, 2015).

Such a cutoff is necessarily arbitrary, and will remain so for the foreseeable future, as the actual values of  $M_{\text{CUT}} \sim -13$  are not only beyond the limit of the existing HST observations, but will also be hard to reach even by JWST observations of lensed reionization sources.

Therefore, it may make sense to explore what the current theory has to say on the specific shape of the galaxy UV luminosity function and possible reasonable values of  $M_{\text{CUT}}$ . In this paper I use numerical simulation of reionization completed under the ‘‘Cosmic Reionization On Computers’’ (CROC) project as a theoretical tool. CROC simulations are a suitable tool for this purpose, since they, currently, match all existing observational constraints, from galactic properties such as luminosity functions, UV slopes, and IR excesses, to the properties of the IGM at  $z < 6$  such as full PDFs of Gunn-Peterson optical depth in several redshift bins, flux gap statistics, etc (Gnedin & Kaurov 2014; Khakhaleva-Li & Gnedin 2016; Gnedin et al. 2016). They are also comparable to or

exceeding other modern, fully self-consistent simulations of reionization in mass and spatial resolution and in the box size.

CROC simulations are also useful for modeling galaxy UV luminosity functions, since their latest series has been shown to provide numerically (albeit weakly) converged results (Gnedin 2016). Hence, numerical effects are under control in CROC simulations and do not exceed 20% for galaxy luminosity functions at all redshifts.

The full details of numerical setups of CROC simulations are presented in Gnedin (2014) and Gnedin (2016), and I do not repeat them here for the sake of brevity. In this paper I use a new ‘‘Cayman’’ series of simulations that maintain spatial resolution fixed in physical units (rather than in comoving units, as the first generation of CROC runs) and include weak convergence corrections from Gnedin (2016) that compensate numerical results for finite spatial and mass resolution and make them approximately resolution independent (and equal to the fully numerically converged values). In the rest of the paper simulation sets are labeled in the following way: the label starts with the box size (B20 standing for the  $20h^{-1}$  Mpc box size) followed by the mass resolution (MR for ‘‘medium’’ and HR for ‘‘high’’ mass resolution, which stand for  $512^3$  and  $1024^3$  initial grids in  $20h^{-1}$  Mpc boxes and proportionally larger grids in larger boxes respectively) and concluded with the spatial resolution (R100 standing for the spatial resolution of 100 pc in physical units).

## 2. THE FAINT END OF THE GALAXY UV LUMINOSITY FUNCTION

Galaxy UV luminosity functions at a range of redshifts are a primary reionization observable, and provide stringent constraints on the properties of reionization sources. In Figure 1 I show galaxy luminosity functions at  $z \gtrsim 6$  and their logarithmic slopes, as well as their Schechter function fits, for the fiducial set of 6 independent realizations of the B20MR.R100 box. Simulated luminosity functions peak at  $M_{1500} \sim -12$  and drop rapidly at lower magnitudes. The specific shape of this drop is *not* a reliable prediction of the simulations - it depends on the details of the star formation algorithm, and, in particular, on the adopted minimum mass of a stellar particle. These details, however, do not affect the total luminosity density or the shape of the luminosity function at  $M_{1500} < -12$ .

A parameter, which is of a particular interest to analyti-

<sup>1</sup> Particle Astrophysics Center, Fermi National Accelerator Laboratory, Batavia, IL 60510, USA; gnedin@fnal.gov

<sup>2</sup> Kavli Institute for Cosmological Physics, The University of Chicago, Chicago, IL 60637 USA;

<sup>3</sup> Department of Astronomy & Astrophysics, The University of Chicago, Chicago, IL 60637 USA

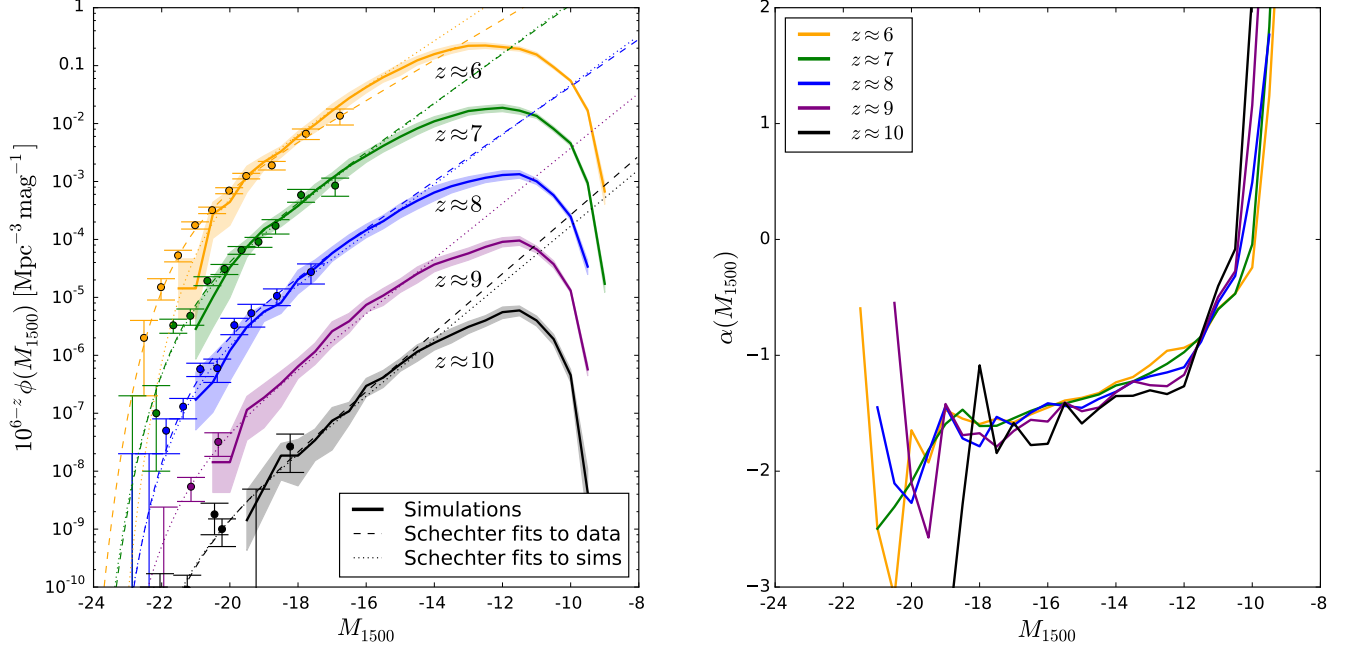


FIG. 1.— Galaxy UV luminosity functions (left) and their local slopes (right) at 5 different redshifts for the fiducial B20MR.R100 simulation set. Points with error-bars and dotted lines in the left panel are observational data and their Schechter function fits from Bouwens et al. (2015), while the dashed lines are Schechter function fits to the simulation results in the interval  $-22 < M_{1500} < -16$ .

cal modeling, is the limiting magnitude  $M_{\text{CUT}}$  to which the Schechter fit to the luminosity function must be integrated to recover the total luminosity density. To illustrate its role, I show in Figure 2 cumulative luminosity functions for 3 different simulation sets with varied spatial and mass resolution. Actual model luminosity functions start deviating from their Schechter fits at  $M_{1500} \sim -14$ , and reach their asymptotic values at  $M_{1500} > -12$ . One can then define the cutoff luminosity  $L_{\text{CUT}}$  for the Schechter function fit so that the total luminosity density  $j_{\text{UV}}$  in the actual simulated luminosity function and

its Schechter fit are equal,

$$j_{\text{UV}} \equiv \int_0^\infty \phi_{\text{SIM}}(L) L dL = \int_{L_{\text{CUT}}}^\infty \phi_{\text{SCH}}(L) L dL. \quad (1)$$

Corresponding magnitude cuts are plotted in Figure 3 for the three simulation sets used above, and two larger box sets (to test the effect of the box size). About 1 magnitude difference between different simulation sets should be treated as the estimate of the theoretical uncertainty, as all sets are weakly numerically converged (Gnedin 2016); however, some modest, below 20%, residual dependence on the mass and spatial resolution and on the box size remains. The cutoff magnitude is slightly redshift dependent, but that dependence is too mild to significantly affect ionization history modeling discussed below.

### 3. IONIZATION HISTORY MODELING

Galaxy UV luminosity functions are often used in modeling reionization history of the universe. The simplest form of such modeling was introduced by Madau et al. (1999); it is based on a single evolution equation for the filling factor of ionized gas  $Q_{\text{HII}}$ ,

$$\frac{dQ_{\text{HII}}}{dt} = \frac{\dot{n}_{\text{ion}}}{n_{\text{H}}} - \frac{Q_{\text{HII}}}{\bar{t}_{\text{REC}}}, \quad (2)$$

where  $\dot{n}_{\text{ion}}$  is the globally averaged rate of production of hydrogen ionizing photons,  $n_{\text{H}}$  is the averaged hydrogen nuclei density, and  $\bar{t}_{\text{REC}}$  is the harmonically averaged, ionizing gas mass-weighted hydrogen recombination time,

$$\bar{t}_{\text{REC}} \equiv \langle x_i / t_{\text{REC}} \rangle_M / \langle x_i \rangle_M. \quad (3)$$

Madau et al. (1999) type modeling remains a useful tool despite its simplicity; in particular, I use hereafter the work of Robertson et al. (2015) as one of the most recent and widely regarded analytical models of reionization.

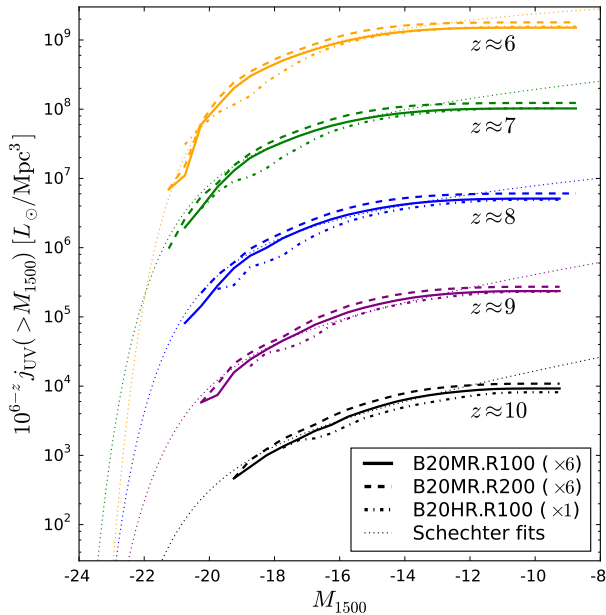


FIG. 2.— Cumulative galaxy UV luminosity functions for 3 different simulation sets with different mass and spatial resolution and Schechter function fits to the fiducial set B20MR.R100.

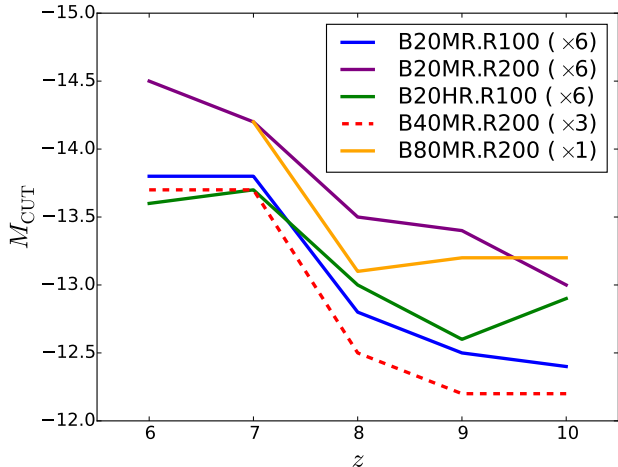


FIG. 3.— Cutoff magnitudes  $M_{\text{CUT}}$  to which Schechter function fits need to be integrated to recover the correct total UV luminosity density, as functions of redshift, for several simulation sets.

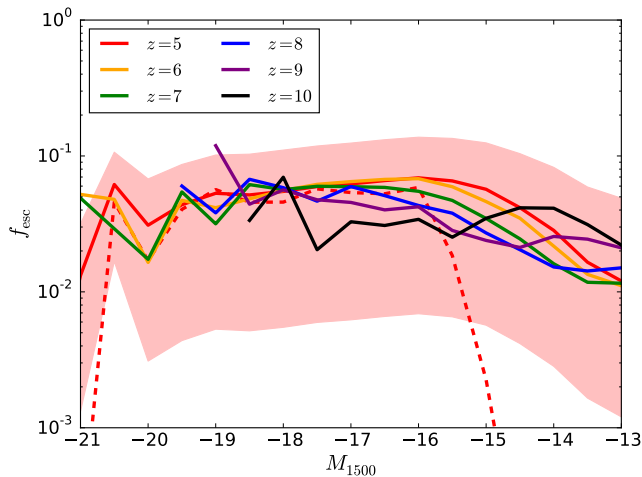


FIG. 4.— Average escape fractions of ionizing radiation [see] for the exact definition]ng:gkc08 as functions of galaxy UV luminosity at several redshifts (solid lines). At  $z = 5$  the dashed line also shows the median escape fraction (to illustrate the complexity of the whole distribution), and the colored band tracks the rms scatter around the mean.

Equation 2 has one major limitation: it assumes that all photons are expended on ionizing general IGM, hence ignoring ionizing photon loss in Lyman limit systems (Furlanetto & Oh 2005; Furlanetto & Mesinger 2009; Kaurov & Gnedin 2013), which becomes important closer to the end of reionization.

The term  $\dot{n}_{\text{ion}}$  is commonly evaluated as (Robertson et al. 2015)

$$\dot{n}_{\text{ion}} = f_{\text{ESC}}^{\text{eff}} \xi_{\text{ION}} \dot{\rho}_* = f_{\text{ESC}} \xi_{\text{ION}} \kappa_{\text{UV}} j_{\text{UV}}, \quad (4)$$

where  $f_{\text{ESC}}^{\text{eff}}$  is the “effective” escape fraction of ionizing photons,  $\xi_{\text{ION}}$  is the ionizing photon production efficiency per unit star formation rate,  $\kappa_{\text{UV}}$  is the conversion factor from UV luminosity to star formation rate, and  $j_{\text{UV}}$  is the UV luminosity density from Equation (1).

Computing escape fraction in a simulation is usually a thankless task, since simulated, used in the analytical modeling, and observationally constrained escape fractions are all different quantities and can not be meaningfully compared to each other without additional, often poorly justified, assumptions (Gnedin et al. 2008). However, as an illustration

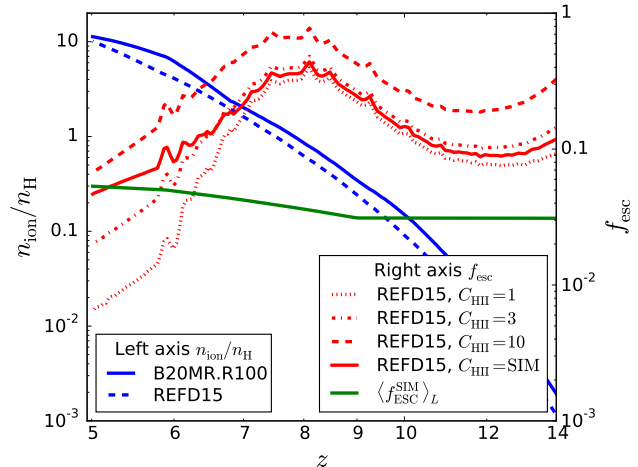


FIG. 5.— Evolution of the number of ionizing photons per hydrogen nucleus (left axis), as actually produced in the simulations (solid blue line) and as computed from the globally averaged star formation rate using Equation (4) (4-dashed blue line) with the choice of parameters from Robertson et al. (2015). The right axis is for the effective escape fractions at several values of the assumed clumping factor in the Robertson et al. (2015) model. Solid red line assumes the clumping factor from the actual simulations Kaurov & Gnedin (Fig. 6 from 2015), and the solid green function tracks the true luminosity-weighted average escape fraction from the simulations. The rapid drop in the effective escape fractions at  $z \lesssim 8$  indicates the breakdown of a simple model of Equation 2.

and to help to elaborate the discussion below, I show in Figure 4 the escape fractions of ionizing radiation (i.e., not the monochromatic escape fraction at  $912\text{\AA}$ , but the one fully integrated over the ionizing radiation spectrum) in the fiducial B20MR.R100 simulation set at several redshift, averaged in bins of galactic magnitudes. Average escape fractions do not vary much with galaxy luminosity, and the scatter is large, making a commonly made in the analytical modeling assumption of constant escape fraction not a bad one. Luminosity weighted globally averaged escape fraction vary by less than a factor of 2 between  $z \sim -10$  and  $z = 5$ .

To explore the connection with the analytical modeling even further, I show in Figure 5 both the production rate of ionizing photons per hydrogen nucleus  $\dot{n}_{\text{ion}}/n_{\text{H}}$  (left axis) and the effective escape fraction one has to use in Equation (4) in order to reproduce the actual simulated ionization history as a solution of Equation (2) for several values of the assumed clumping factor that enters the definition of  $\bar{\tau}_{\text{REC}}$  - the specific values of other parameters are set exactly as in Robertson et al. (2015).

The ionizing photon production rate can be computed in two ways: either extracted directly from the simulations or converted from the global star formation rate via Equation (4). Both approaches give values that differ by less than 25%, and the difference is primarily due to the factor  $\xi_{\text{ION}}$  - while Robertson et al. (2015) assume a fixed value for this quantity, in the simulations each stellar particle uses its own, metallicity-dependent factor  $\xi_{\text{ION}}$ , as computed by Starburst99 code (see Gnedin 2014, for details). This difference and the difference in the assumed values for  $\kappa_{\text{UV}}$  are the reason behind the approximately constant fractional offset in the values of the escape fraction from the simulation and the effective escape fraction in the analytical model at early times.

The actually measured in the simulations globally averaged, luminosity-weighted escape fractions do not evolve much (a solid green line in Fig. 5). However, the effective escape frac-

tions  $f_{\text{ESC}}^{\text{eff}}$  one needs to use in Equations (2) and (4) vary in a non-trivial way, first increasing by a factor of 3 at  $z \sim 8$  and later dropping rapidly by an order of magnitude or more. Such a complex behavior, not mirrored in the actually simulated escape fractions, is, therefore, a manifestation of the limitations of Equation (2).

The late time ( $z \lesssim 8$ ) discrepancy is easy to understand. As the mean free path of ionizing photons increases, the process of reionization is slowed down by the progressively larger fraction of ionizing photons being lost in Lyman limit systems (until, at the end of reionization, this fraction becomes 100%). Since Equation (2) does not take this loss into account, a reduced effective escape fraction is needed to keep the universe less ionized than what one would expect if no photons were lost in Lyman limit systems. In fact, the redshift-dependent form for the effective escape fraction from equation (15) of Robertson et al. (2013b) captures this regime well.

An increase in the effective escape fraction at intermediate redshifts ( $z \sim 8$ ) is harder to interpret. One possible explanation is the cross-correlation between the recombination time (or, rather, the clumping factor) and the distribution of ionized gas - ionized gas has higher pressure, less small-scale structure, and hence is less clumped than the same gas before it became ionized. However, this decrease in the clumping factor takes time, and until the extra small-scale structure is erased, freshly ionized gas remains more clumped than on average. A higher escape fraction would be needed to compensate for the additional clumping in the gas.

Formally, Equation (2) accounts for this effect by defining  $\bar{\tau}_{\text{REC}}$  in Equation (3) as appropriately averaged. However, in practice, this is rarely accounted for, and most commonly a simple ansatz  $\bar{\tau}_{\text{REC}} \propto n_{\text{H}}^{-1}$  is adopted (as in Robertson et al. 2015).

#### 4. CONCLUSIONS

Galaxy UV luminosity functions, as modeled by CROC simulations, agree well with the existing observational measurements. When fitted with a Schechter functional form, they

require the cutoff magnitude in the fitting function between -12 and -14, with only slight redshift dependence, in good agreement with assumptions made in the Madau et al. (1999) style analytical modeling using Equation (2) (c.f. Robertson et al. 2015, as the latest example of such modeling).

However, a more serious problem with this type of modeling is in the adopted assumptions about the effective escape fraction of ionizing radiation. While actual escape fractions in the simulations are approximately constant in time and with galaxy luminosity, intrinsic limitations of Equation (2) make the effective escape fraction one has to use in Equation (4) strongly and non-trivially redshift-dependent. One of these limitations is not accounting for photon loss in the Lyman limit systems, which causes a rapid drop in the effective escape fraction at the end of reionization.

A smaller, but still significant variation in the effective escape fraction takes place in the middle of reionization, at  $z \sim 8$ . An increase of about a factor of 2 to 3 is required to match the simulated results, and the exact cause of this discrepancy is far from obvious. One possible culprit is the omission of correlations between gas clumping and its ionization state, but the full exploration of the discrepancy is beyond the scope of this short paper.

I am grateful to Brant Robertson for valuable comments on the earlier draft. CROC simulations have been performed on the University of Chicago Research Computing Center cluster “Midway”, on National Energy Research Supercomputing Center (NERSC) supercomputers “Cori” and “Edison”, and on the Argonne Leadership Computing Facility supercomputer “Mira”. An award of computer time was provided by the Innovative and Novel Computational Impact on Theory and Experiment (INCITE) program. This research used resources of the Argonne Leadership Computing Facility, which is a DOE Office of Science User Facility supported under Contract DE-AC02-06CH11357.

#### REFERENCES

- Atek, H., Richard, J., Jauzac, M., Kneib, J.-P., Natarajan, P., Limousin, M., Schaerer, D., Jullo, E., Ebeling, H., Egami, E., & Clement, B. 2015a, ArXiv e-prints
- Atek, H., Richard, J., Kneib, J.-P., Jauzac, M., Schaerer, D., Clement, B., Limousin, M., Jullo, E., Natarajan, P., Egami, E., & Ebeling, H. 2015b, ApJ, 800, 18
- Bouwens, R. J., Illingworth, G. D., Oesch, P. A., Labbé, I., Trenti, M., van Dokkum, P., Franx, M., Stiavelli, M., Carollo, C. M., Magee, D., & Gonzalez, V. 2011, ApJ, 737, 90
- Bouwens, R. J., Illingworth, G. D., Oesch, P. A., Trenti, M., Labbé, I., Bradley, L., Carollo, M., van Dokkum, P. G., Gonzalez, V., Holwerda, B., Franx, M., Spitler, L., Smit, R., & Magee, D. 2015, ApJ, 803, 34
- Bowler, R. A. A., Dunlop, J. S., McLure, R. J., Rogers, A. B., McCracken, H. J., Milvang-Jensen, B., Furusawa, H., Fynbo, J. P. U., Taniguchi, Y., Afonso, J., Bremer, M. N., & Le Fèvre, O. 2014, MNRAS, 440, 2810
- Bradley, L. D., Trenti, M., Oesch, P. A., Stiavelli, M., Treu, T., Bouwens, R. J., Shull, J. M., Holwerda, B. W., & Pirzkal, N. 2012, ApJ, 760, 108
- Finkelstein, S. L., Ryan, Jr., R. E., Papovich, C., Dickinson, M., Song, M., Somerville, R. S., Ferguson, H. C., Salmon, B., Giavalisco, M., Koekemoer, A. M., Ashby, M. L. N., Behroozi, P., Castellano, M., Dunlop, J. S., Faber, S. M., Fazio, G. G., Fontana, A., Grogin, N. A., Hathi, N., Jaacks, J., Kocevski, D. D., Livermore, R., McLure, R. J., Merlin, E., Mobasher, B., Newman, J. A., Rafelski, M., Tilvi, V., & Willner, S. P. 2015, ApJ, 810, 71
- Furlanetto, S. R. & Mesinger, A. 2009, MNRAS, 394, 1667
- Furlanetto, S. R. & Oh, S. P. 2005, MNRAS, 363, 1031
- Gnedin, N. Y. 2014, ApJ, 793, 29
- . 2016, ArXiv e-prints
- Gnedin, N. Y., Becker, G. D., & Fan, X. 2016, in preparation
- Gnedin, N. Y. & Kaurov, A. A. 2014, ApJ, 793, 30
- Gnedin, N. Y., Kravtsov, A. V., & Chen, H.-W. 2008, ApJ, 672, 765
- Kaurov, A. A. & Gnedin, N. Y. 2013, ApJ, 771, 35
- . 2015, ApJ, 810, 154
- Khakhaleva-Li, Z. & Gnedin, N. Y. 2016, ArXiv e-prints
- Madau, P., Haardt, F., & Rees, M. J. 1999, ApJ, 514, 648
- Oesch, P. A., Bouwens, R. J., Illingworth, G. D., Gonzalez, V., Trenti, M., van Dokkum, P. G., Franx, M., Labbé, I., Carollo, C. M., & Magee, D. 2012, ApJ, 759, 135
- Oesch, P. A., Bouwens, R. J., Illingworth, G. D., Labbé, I., Franx, M., van Dokkum, P. G., Trenti, M., Stiavelli, M., Gonzalez, V., & Magee, D. 2013, ApJ, 773, 75
- Oesch, P. A., Bouwens, R. J., Illingworth, G. D., Labbé, I., Smit, R., Franx, M., van Dokkum, P. G., Momcheva, I., Ashby, M. L. N., Fazio, G. G., Huang, J.-S., Willner, S. P., Gonzalez, V., Magee, D., Trenti, M., Brammer, G. B., Skelton, R. E., & Spitler, L. R. 2014, ApJ, 786, 108
- Robertson, B. E., Ellis, R. S., Furlanetto, S. R., & Dunlop, J. S. 2015, ApJ, 802, L19
- Robertson, B. E., Furlanetto, S. R., Schneider, E., Charlot, S., Ellis, R. S., Stark, D. P., McLure, R. J., Dunlop, J. S., Koekemoer, A., Schenker, M. A., Ouchi, M., Ono, Y., Curtis-Lake, E., Rogers, A. B., Bowler, R. A. A., & Cirasuolo, M. 2013a, ArXiv e-prints
- . 2013b, ApJ, 768, 71
- Schenker, M. A., Robertson, B. E., Ellis, R. S., Ono, Y., McLure, R. J., Dunlop, J. S., Koekemoer, A., Bowler, R. A. A., Ouchi, M., Curtis-Lake, E., Rogers, A. B., Schneider, E., Charlot, S., Stark, D. P., Furlanetto, S. R., & Cirasuolo, M. 2013, ApJ, 768, 196

Song, M., Finkelstein, S. L., Ashby, M. L. N., Grazian, A., Lu, Y., Papovich, C., Salmon, B., Somerville, R. S., Dickinson, M., Duncan, K., Faber, S. M., Fazio, G. G., Ferguson, H. C., Fontana, A., Guo, Y., Hathi, N., Lee, S.-K., Merlin, E., & Willner, S. P. 2015, ArXiv e-prints  
Weisz, D. R., Johnson, B. D., & Conroy, C. 2014, ApJ, 794, L3

Willott, C. J., McLure, R. J., Hibon, P., Bielby, R., McCracken, H. J., Kneib, J.-P., Ilbert, O., Bonfield, D. G., Bruce, V. A., & Jarvis, M. J. 2013, AJ, 145, 4